PHYSICAL REVIEW B VOLUME 48, NUMBER 19 15 NOVEMBER 1993-I

Simplified microscopic model for electron–optical-phonon interactions in quantum wells

A. R. Bhatt and K. W. Kim
Department of Electrical and Computer Engineering, North Carolina State University, Raleigh, North Carolina 27695-7911

M. A. Stroscio
U.S. Army Research Office, P.O. Box 12211, Research Triangle Park, North Carolina 27709-2211

J. M. Higman*
Beckman Institute, University of Illinois, Urbana, Illinois 61801
(Received 17 May 1993)

A simplified microscopic model of optical phonons in dimensionally confined structures is formulated and applied to calculate electron–optical-phonon scattering rates in GaAs/AlAs quantum wells. For this simplified model which circumvents performing a complicated *ab initio* calculation of the force constants at the interface, it is demonstrated that the resulting dispersion relation and scattering rates for electron–optical-phonon interactions agree very well with those obtained from detailed *ab initio* studies. It is also shown that for GaAs/AlAs structures, the macroscopic dielectric continuum model provides a good approximation to the scattering rate predicted by the microscopic models.

The electronic and optical properties of semiconductor superlattices (SL's) and quantum wells (QW's) have been investigated extensively. A principal advantage of using such heterostructures results from the ability to tailor the electronic and optical properties of the structures for realizing a potentially vast array of high-performance electronic and optoelectronic devices. To fully understand and utilize the properties of these nanometer-scale heterostructures, it is necessary to develop formalisms for studying confinement effects as well as picosecond and subpicosecond processes. It has been known for many years that the scattering by polar–optical-phonon modes is an important energy-loss mechanism for electrons in a wide variety of III-V semiconductor devices. However, effects of confinement on these phonon modes have been investigated extensively only in the past several years.

In recent years, a number of models has been put forward to explain electron–optical-phonon interactions in reduced dimensional systems. They can be broadly classified in two categories: macroscopic[1–9] and microscopic.[10–12] Macroscopic models ignore the effect of individual layers of atoms but they have the considerable advantage of making the interaction calculation very simple. Among these macroscopic models are the dielectric continuum model[1–5] (slab model, which uses purely electrostatic boundary conditions), hydrodynamic model,[7] hybrid model,[8] and a recent dispersive continuum treatment of Nash.[9] In some parameter regimes, these models are fairly accurate and provide good estimates of energy-loss rates. However, scaling of the electron–optical-phonon interaction with diminishing device length presents a serious challenge to the accurate use of such models. As a result, there has recently been an increasing need for more rigorous analysis and detailed knowledge of electron–optical-phonon interactions in reduced dimensional systems. This has been the main motivation for the emergence of *ab initio* microscopic models.[12] Though such models provide the most accurate analysis of the structure, they have not been used extensively. This can be attributed to the fact that the *ab initio* microscopic analysis involves very arduous and time consuming first-principle calculations of lattice dynamics[13,14] rather than employing adjustable parameters.[15–17]

Precise *ab initio* calculations of force constants at the interface may not be essential for most of the heterostructures except those involving extremely thin layers. It is well known that even a simple linear-chain model with nearest-neighbor force constants can predict the zone-center LO-phonon frequencies in a SL with a reasonable accuracy except in the cases where layers are single monolayer thick. Such an approximate model is based on the assumption that atomic-force constants at heterojunction interfaces are identical to those of the bulk or of uniform pseudomorphic layers. In a qualitative analysis of the effect of varying force constants at the heterojunction interfaces of a strained layer, short-period, GaAs/GaP SL with two monolayers per SL layer, it was also found that frequencies of the confined phonon modes are only weakly dependent on the variations in the interfacial force constants.[18] The variation in interfacial force constants by values as extreme as 10% results in less than about a 2% change in the frequencies of confined phonon modes. It should be noted that as a practical matter, changes in the frequencies of the confined LO-phonon modes will be considerably less than 2%, since in most SL's and QW's the ratio of the number of bonds at the interfaces to the number of bonds one or more monolayers away from the interfaces is less than that for the case where each layer is two monolayers thick.

Based on the results of Ref. 18, as well as on supporting observations from other investigators,[19] we have formulated a simplified microscopic model which facilitates the accurate modeling of confined and interface phonons without *ab initio* calculations of force constants. The valence-shell model developed by Kunc and Nielson for bulk[20] has been extended for the SL/QW structures. In-

0163-1829/93/48(19)/14671(4)/$06.00

terpolation of the force constants at the heterointerfaces and a periodic-boundary condition have been applied as suggested by Yip and Chang.[15] The calculated phonon dispersion and atomic displacements have been used to derive the interaction Hamiltonian and the electron–optical-phonon scattering rates in SL/QW heterostructures. As will be demonstrated below, this simplified model provides an excellent approximation to the fully microscopic model. As a specific example in this study, we consider GaAs/AlAs SL/QW structures grown in the (001) direction.

The dispersion relation can be obtained from the dynamical matrix constructed using our modified shell model. Three types of interactions are included: the core-to-core (Φ^R) potential, the shell-to-core (Φ^T) potential, and the shell-to-shell (Φ^S) potential. The corresponding dynamical matrices are[20]

$$R_{\alpha\beta}(j,j',\mathbf{q})=\sum_{l-l'}\Phi^R_{\alpha\beta}(l-l',j,j')e^{i\mathbf{q}\cdot[\mathbf{z}(l,j)-\mathbf{z}(l',j')]}, \quad (1)$$

$$S_{\alpha\beta}(j,j',\mathbf{q})=\sum_{l-l'}\Phi^S_{\alpha\beta}(l-l',j,j')e^{i\mathbf{q}\cdot[\mathbf{z}(l,j)-\mathbf{z}(l',j')]}, \quad (2)$$

$$T_{\alpha\beta}(j,j',\mathbf{q})=\sum_{l-l'}\Phi^T_{\alpha\beta}(l-l',j,j')e^{i\mathbf{q}\cdot[\mathbf{z}(l,j)-\mathbf{z}(l',j')]}, \quad (3)$$

where j (j') denotes the atom in the cell and its type, l (l') represents the unit cell, $\mathbf{z}(l,j)$ [$\mathbf{z}(l',j')$] is the position of the jth (j'th) atom in the lth (l'th) cell, and α,β denote the direction. Along with these matrices, we also need to use "effective" shell-shell interactions as,[20]

$$\Delta_{\alpha\beta}(j,j',\mathbf{q})=S_{\alpha\beta}(j,j',\mathbf{q})+\delta_{\alpha\beta}\delta_{jj'}[K_j+T_{\alpha\alpha}(j,j,0)-S_{\alpha\alpha}(j,j,0)], \quad (4)$$

where K_j represents the internal core-shell spring. The equation of motion can be found using the following matrix equations:[20]

$$\omega^2 M\mathbf{u}=(R-ZBZ)\mathbf{u}+(T-ZBY)\mathbf{w}, \quad (5)$$

and

$$0=(T^+-YBZ)\mathbf{u}+(\Delta-YBY)\mathbf{w}, \quad (6)$$

where M, Z, Y, and B are matrices of masses, ionic charges, shell charges, and the real part of Coulomb interaction, respectively, as specified in Ref. 20. Here $\mathbf{u}$ and $\mathbf{w}$ stand for the amplitudes $\mathbf{u}(\mathbf{q})$ and $\mathbf{w}(\mathbf{q})$ of the core and relative-shell displacement, respectively, which may given as

$$u^\nu_\alpha(lj)=u^\nu_\alpha(j,\mathbf{q})\exp[-i\omega_\nu(\mathbf{q})t+i\mathbf{q}\cdot\mathbf{z}(lj)], \quad (7)$$

and

$$w^\nu_\alpha(lj)=w^\nu_\alpha(j,\mathbf{q})\exp[-i\omega_\nu(\mathbf{q})t+i\mathbf{q}\cdot\mathbf{z}(lj)], \quad (8)$$

where ν represents the phonon mode index. From Eqs. (5) and (6), it is clear that the eigenvalue problem reduces to

$$[C(\mathbf{q})-\omega^2 I]\mathbf{e}=0, \quad (9)$$

with

$$C(q)=M^{-1/2}[(R-ZBZ)-(T-ZBY)\times(\Delta-YBY)^{-1}\times(T^+-YBZ)]M^{-1/2}. \quad (10)$$

In a bulk zinc-blende structure, this equation results in six eigenvalues, ω_ν, and six eigenvectors, $\mathbf{e}_\nu$, for a given $\mathbf{q}$. The corresponding phonon-dispersion relations and displacements are obtained directly from the expressions given above. The results are essentially the same as those calculated in a simple linear-chain model with nearest-neighbor force constants. The long-range Coulomb interaction turns out to be less important because its force range is effectively reduced and its effect is only to slightly modify the nearest-neighbor and next-nearest-neighbor force constants.[16] The parameters used in this study for three types of interaction [i.e., R, S, and T in Eqs. (1)–(3)] are as listed in Table I; these parameters yield an excellent description of bulk-phonon characteristics for both GaAs and AlAs. All the other required parameters can be found in the literature.[11,15,16,20] Extension of this approach to a SL is rather straightforward. In a SL grown in the (001) direction, the symmetry consideration along the x-y plane is maintained, while the translational period in the z direction needs to be modified. We define a SL unit cell L along the $\mathbf{z}$ direction which consists of n unit cells of each material and a SL wave vector $\mathbf{q}_z$. Hence, along $\mathbf{z}$ direction all summations need to be performed over all unit cells of the SL cell. Interactions up to the second nearest neighbors are taken into account. As mentioned before, the bulk parameters are used in each layer except at the heterointerfaces where the interpolated force constants are adopted. The resulting dynamical matrices provide all of the SL eigenfrequencies and eigenvectors for phonon modes.

Figure 1 shows the phonon-dispersion relation for a (001) oriented $(GaAs)_{20}/(AlAs)_{20}$ SL along the in-plane (100) direction and also as a function of angle θ between the direction of wave vector $\mathbf{q}$ and the in-plane direction for vanishingly small q; θ ranges from 0 to $\pi/2$. Two clearly defined GaAs-like and AlAs-like frequency ranges are apparent in Fig. 1. Along with LO and TO modes, it

TABLE I. Converted parameters used in this study for the three types of interaction [i.e., R, S, and T in Eqs. (1)–(3)]. A, B, $C1$, $D1$, $E1$, $F1$, $C2$, $D2$, $E2$, and $F2$ are as defined in Ref. 19 and determined by fitting the bulk GaAs and AlAs phonon-dispersion relations.

	Converted parameters					
	GaAs			AlAs		
	R	S	T	R	S	T
A	−19.67	−24.92	−19.67	−20.13	−23.87	−20.13
B	−4.44	3.31	−0.847	−4.31	3.39	−0.892
$C1$	0.817	1.034	0.817	0.799	1.011	0.799
$D1$	−0.736	0.933	−0.736	−0.801	0.933	0.801
$E1$	−0.550	−0.697	−0.550	−0.610	−0.701	−0.610
$F1$	1.942	2.461	1.942	2.42	3.643	2.42
$C2$	0.817	1.034	0.817	−0.799	1.011	0.799
$D2$	0.736	−0.933	−0.736	0.801	−0.933	−0.801
$E2$	0.550	−0.697	−0.550	0.610	−0.701	−0.610
$F2$	1.942	2.461	1.942	2.42	3.643	2.42

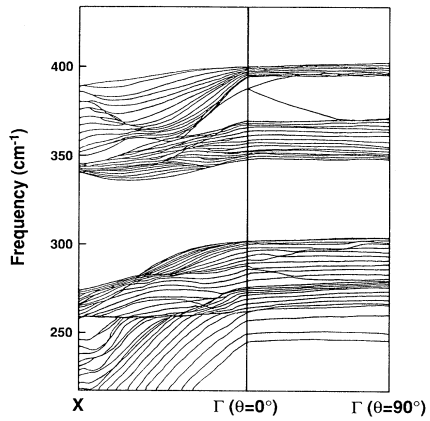

FIG. 1. Phonon dispersion of a (001)-oriented $(GaAs)_{20}/(AlAS)_{20}$ SL along the in-plane direction and as a function of angle θ between the direction of wave vector $\mathbf{q}$ and the in-plane direction for vanishing small q.

should be noted that the two "AlAs-like" principal modes and two "GaAs-like" principal modes take the limit of the well known "interface modes" of the dielectric continuum model over a portion of the domain of Fig. 1. Another feature of interest is the anticrossing of the modes in the right-hand panel (i.e., angular dependence).[15] (Similar anticrossing characteristics of the modes have been observed in Refs. 8 and 9 as well.) Compared to the results from the *ab initio* approach,[12] it is clear that our simple microscopic model can describe detailed characteristics of phonon dynamics accurately at the current dimension. As the layer thickness decreases, however, the accuracy of our model may suffer due to the assumptions made for the interface force constants. As an indication for validity of our model, the LO-phonon frequencies have been calculated for the $(GaAs)_m/(AlAs)_n$ SL's with $m=n$ ranging from 1 to 4. In this comparison, our results match well with the observed LO-phonon frequencies[21] for $m=n\geq 2$ (within 3 cm^{-1}). For the monolayer case, the agreement between the experimental data and our microscopic model is not as good, but it is considerably better than those calculated by using the simple linear-chain model.[21] To study this case accurately, one will have to employ first-principle calculations using *ab initio* calculations at the heterostructure interface. Nevertheless, our model should provide excellent results for the great majority of device applications since layer thicknesses generally exceed one monolayer.

The Hamiltonian for the polar electron–optical-phonon interaction in a single QW can be found from the potential given as[12]

$$\phi(z)=\sum_{n,\nu,q_\parallel} U^\nu e_n^* \left[\frac{iq_\parallel u_{nz}^\nu(q_\parallel)}{|q_\parallel|}-u_{nz}^\nu(q_\parallel)\mathrm{sgn}(z-z_n)\right] \times e^{-(q_\parallel|z-z_n|)} \tag{11}$$

with

$$U^\nu=\frac{1}{2\Omega_\parallel\epsilon_\infty}\left[\frac{\hbar}{2N_0\omega_\nu(q_\parallel)}\right]^{1/2}, \tag{12}$$

where e_n^* is effective charge ($2.07|e|$ for GaAs and $2.17|e|$ for AlAs), n ranges all the N_0 lattice points in the normalization volume, and $\Omega_\parallel$ is the area of two-dimensional unit cell. Based on the Fermi golden rule, the scattering rate for the electron–optical-phonon interaction can be obtained as

$$\Gamma(i,j)=(2\pi/\hbar)|\langle f|H|i\rangle|^2\delta(E_f-E_i)\,, \tag{13}$$

where i and f denote the initial and final states of the crystal, respectively, and H is the interaction Hamiltonian given by $-e\phi$, where e is the electron charge and ϕ is the electrostatic potential associated with the lattice vibration as given above. Accordingly,

$$\Gamma_{ij}(k_\parallel)=\frac{2\pi e^2}{\hbar}\sum_{k'_\parallel,\nu}|G_{ij}(q_\parallel,\nu)|^2(N+\tfrac{1}{2}\pm\tfrac{1}{2}) \times\delta\left[\frac{\hbar^2k_\parallel^2}{2m^*}-\frac{\hbar^2k'^2_\parallel}{2m^*}\mp\hbar\omega^*\right], \tag{14}$$

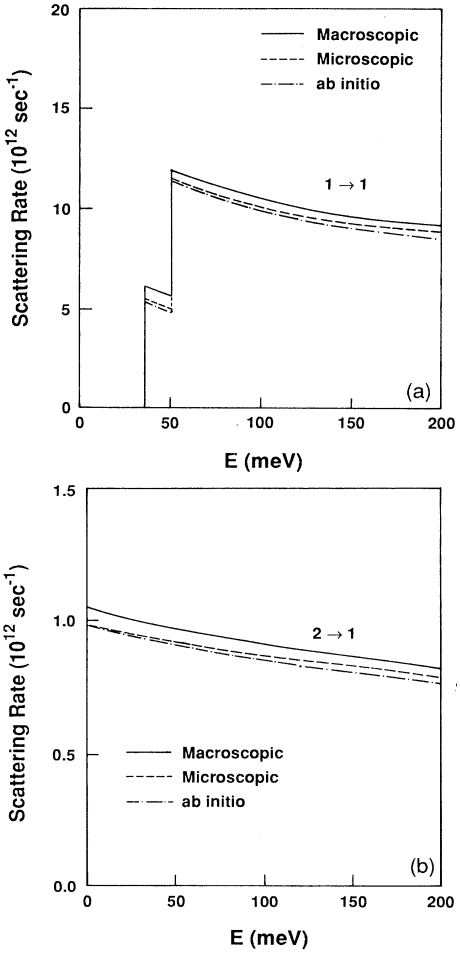

FIG. 2. Scattering rates by electron–optical-phonon interaction as a function of electron energy in a GaAs/AlAs single QW structure with a 20-monolayer GaAs well at 300 K. The results in (a) present the intrasubband transition rates of the lowest subband ($1\rightarrow 1$), while the data in (b) show the intersubband transition rates from the second lowest to the lowest subband ($2\rightarrow 1$).

where $\hbar\omega^* = \hbar\omega_\nu(q_\parallel) \pm (E_j - E_i)$ and $k_\parallel = k'_\parallel \pm q_\parallel$. Also, the form factor G_{ij} is given by

$$G_{ij}(q_\parallel, \nu) = \int \zeta_i^*(z)\zeta_j(z)\phi(z)dz \ , \tag{15}$$

where ζ_i and ζ_j are the electronic envelope functions for subbands i and j, respectively. ϕ is the potential associated with the quantized phonon modes. For intrasubband ($i=j$) scattering, G_{ij} is nonzero only for phonons with symmetric potentials and modes of opposite parity do not contribute. For the intersubband scattering, G_{ij} is nonzero for only the modes having opposite parity.

Figure 2 shows the calculation of the scattering rates for the polar electron–optical-phonon interaction based on our method. A GaAs/AlAs single QW structure with a 20-monolayer GaAs well is considered for the $1 \rightarrow 1$ (intrasubband) and $2 \rightarrow 1$ (intersubband) transitions by phonon emission at 300 K. Electronic envelope functions are obtained from the solutions of the Schrödinger equation within the effective-mass approximation. For purposes of comparison, Fig. 2 also depicts the corresponding rates as obtained using the *ab initio* calculation[12] and the dielectric continuum model. It is observed in our calculation that for intrasubband scattering, the lowest-order and highest frequency, ω_{LO1}, confined mode is the most dominant mode and will dominate over all higher-order modes; similarly, for the case of intersubband scattering, ω_{LO2} is the mode which provides the maximum contribution to the scattering strength. Interface modes also provide sizable contributions. These observations and the scattering rates by our microscopic model are in excellent agreement with the results from the *ab initio* calculation. It is also evident from the figure that the dielectric continuum model overestimates the scattering rate only slightly in this structure (i.e., 20-monolayer QW), as compared to our model.

In Fig. 3 we have studied the $1 \rightarrow 1$ and $2 \rightarrow 1$ scattering rates for different QW widths. The general trend in both intrasubband and intersubband scattering is an increase in the scattering rate with diminishing well width d; however, the rate of increase for the intrasubband scattering case is much higher than that for the intersubband case. The intersubband scattering rate increases by only 10% for the whole range of well widths. Surprisingly, the

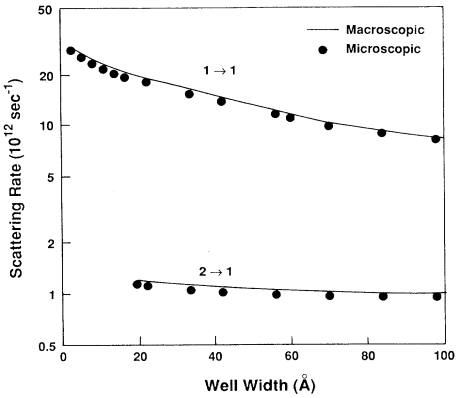

FIG. 3. $1 \rightarrow 1$ and $2 \rightarrow 1$ scattering rates as a function of QW width at 300 K. The electron energy is fixed at 50 meV.

macroscopic approach shows an excellent agreement with the microscopic treatment for well widths as small as 25 Å. As the width of the well is reduced further beyond the range of validity of continuum approximations, the agreement suffers slightly, but still it is well within the acceptable range. We have plotted the intersubband scattering rate for well widths as small as 19 Å. For smaller well widths, the well has only one bound state. There will be a quasibound state outside the well which will contribute to the scattering rate. Though not explicitly shown, the intersubband scattering rate will drop off when the well width becomes smaller than required to maintain at least two bound states. As shown in Ref. 8, the intrasubband and intersubband scattering rates calculated using the hybrid model are also close to those predicted by the dielectric continuum model. Hence we expect that the scattering rate calculations from our microscopic model should form a good agreement with the corresponding results obtained using the hybrid model.

The authors gratefully acknowledge helpful discussions with Dr. G. J. Iafrate and Professor M. A. Littlejohn. This work was supported, in part, by the Office of Naval Research and the U.S. Army Research Office.

*Present address: Advanced Products Research and Development Laboratory, Motorola Inc., Austin, TX 78721.

[1]R. Fuchs and K. L. Kliewer, Phys. Rev. **140**, A2076 (1965); K. L. Kliewer and R. Fuchs, *ibid.* **150**, 573 (1966).
[2]J. J. Licari and R. Evrard, Phys. Rev. B **15**, 2254 (1977).
[3]L. Wendler, Phys. Status Solidi B **129**, 513 (1985).
[4]N. Mori and T. Ando, Phys. Rev. B **40**, 6175 (1989).
[5]K. W. Kim and M. A. Stroscio, J. Appl. Phys. **68**, 6289 (1990).
[6]S. Rudin and T. L. Reinecke, Phys. Rev. B **41**, 7713 (1990).
[7]B. K. Ridley and M. Babiker, Phys. Rev. B **43**, 9096 (1991).
[8]B. K. Ridley, Phys. Rev. B **47**, 4592 (1993); N. C. Constantinou *et al.*, Solid State Commun. **86**, 191 (1993).
[9]K. J. Nash, Phys. Rev. B **46**, 7723 (1992).
[10]K. Huang and B. Zhu, Phys. Rev. B **38**, 377 (1988).
[11]Takuma Tsuchiya, Ph.D. thesis, University of Tokyo, 1990.
[12]E. Molinari *et al.*, Semicond. Sci. Technol. **7**, B67 (1992); H. Rücker *et al.*, Phys. Rev. B **45**, 6747 (1992).
[13]K. Kunc and R. M. Martin, Phys. Rev. Lett **48**, 406 (1982).
[14]S. Baroni *et al.*, Phys. Rev. B **41**, 3870 (1990).
[15]S. K. Yip and Y. C. Chang, Phys. Rev. B **30**, 7037 (1984).
[16]S.-F. Ren *et al.*, Phys. Rev. Lett. **59**, 1841 (1987).
[17]E. Richter and D. Strauch, Solid State Commun. **64**, 867 (1987).
[18]M. A. Stroscio *et al.*, Superlatt. Microstruct. **7**, 115 (1990).
[19]E. Molinari (private communication).
[20]K. Kunc and O. H. Nielson, Comp. Phys. Commun. **17**, 413 (1979): **16**, 181 (1979).
[21]M. Nakayama *et al.*, Solid State Commun. **53**, 493 (1985).